

Effect of helicity and rotation on the free decay of turbulent flows

T. Teitelbaum¹ and P.D. Mininni^{1,2}

¹ *Departamento de Física, Facultad de Ciencias Exactas y Naturales, Universidad de Buenos Aires, Ciudad Universitaria, 1428 Buenos Aires, Argentina.*

² *NCAR, P.O. Box 3000, Boulder, Colorado 80307-3000, U.S.A.*

(Dated: March 2, 2022)

The self-similar decay of energy in a turbulent flow is studied in direct numerical simulations with and without rotation. Two initial conditions are considered: one non-helical (mirror-symmetric), and one with maximal helicity. The results show that, while in the absence of rotation the energy in the helical and non-helical cases decays with the same rate, in rotating flows the helicity content has a major impact on the decay rate. These differences are associated with differences in the energy and helicity cascades when rotation is present. Properties of the structures that arise in the flow at late times in each time are also discussed.

Turbulence is ubiquitous in nature, and many turbulent flows are also rotating. The effect of rotation becomes important when the Rossby number (the ratio of the convective to the Coriolis acceleration) is sufficiently small. Mid-latitude synoptic scales in the atmosphere, stellar convective regions, and turbomachinery are examples of such flows. Helicity (alignment of the velocity and the vorticity) is also important for many processes in astrophysical, geophysical and engineering flows. As an example, helical flows were proposed as the reason for the stability of rotating convective thunderstorms [1].

Studies of isotropic and homogeneous helical turbulence [2, 10] showed that both the helicity and the energy are transferred toward smaller scales with constant fluxes. Moreover, it was observed that the scaling of the energy (Kolmogorov's law) was unchanged by the presence of helicity. As a result, helicity is expected to globally arrest the energy decay, but not to change its self-similar decay rate. Non-helical rotating turbulence has been studied in detail (see e.g., [3] and references therein), but perhaps because of the similarities between the helical and non-helical cases in non-rotating flows, not much attention has been paid to helical rotating turbulence.

The lack of detailed studies of rotating helical flows is remarkable considering the relevance of both helicity and rotation in many astrophysical and geophysical processes. In this work, we study the effect of rotation and of helicity in the self-similar decay of energy in turbulent flows. Even in isotropic and homogeneous turbulence, the law for the decay rate of energy is a matter of debate [4]. It is known that it depends on properties of the infrared energy spectrum (i.e., the spectrum at scales larger than the energy containing scale), and may depend on other statistical properties of the initial conditions. As a result, in this letter we will consider only two flows with the same infrared spectrum and the same energy decay rate in the absence of rotation, and study how the presence of helicity and rotation changes their decay. New decay laws are found for helical rotating flows in numerical simulations. The results are then interpreted in terms of how the energy and helicity cascades are modified when rotation is present, and a phenomenological theory that is in

TABLE I: Parameters used in the simulations: ν is the kinematic viscosity, Ω is the rotation rate, Re is the Reynolds number, Ro is the Rossby number, Ro^ω is the micro-Rossby number, E_k is the Ekman number, and h is the relative helicity of the initial conditions. The values of Re , Ro , Ro^ω , and E_k are given at the time of the peak of dissipation t^* .

Run	ν	Ω	Re	Ro	Ro^ω	E_k	h
A1	1.5×10^{-3}	0	450	—	—	—	0
A2	1.5×10^{-3}	0	600	—	—	—	0.95
A3	1.5×10^{-3}	4	550	0.12	1.28	2.2×10^{-4}	0
A4	1.5×10^{-3}	4	830	0.083	0.8	1.0×10^{-4}	0.95
B1	7×10^{-4}	4	1100	0.12	1.82	1.1×10^{-4}	0
B2	7×10^{-4}	4	1750	0.083	1.15	4.7×10^{-5}	0.95

agreement with the simulations is finally discussed.

The numerical simulations solve the Navier-Stokes equations for an incompressible fluid in a rotating frame,

$$\partial_t \mathbf{u} + \boldsymbol{\omega} \times \mathbf{u} + 2\boldsymbol{\Omega} \times \mathbf{u} = -\nabla \mathcal{P} + \nu \nabla^2 \mathbf{u}, \quad (1)$$

where \mathbf{u} is the velocity field ($\nabla \cdot \mathbf{u} = 0$), $\boldsymbol{\omega} = \nabla \times \mathbf{u}$ is the vorticity, \mathcal{P} is the total pressure (modified by the centrifugal term), and ν is the kinematic viscosity. We chose the rotation axis to be in the z direction, $\boldsymbol{\Omega} = \Omega \hat{z}$, with Ω the rotation frequency. Our integration domain is a periodic box of length 2π . Two sets of runs were done at resolutions of 256^3 (set A) and 512^3 grid points (set B) using a pseudo spectral code. The parameters for all the runs are listed in Table I.

To simulate systems with different amount of relative initial helicity ($h = H / \langle |\mathbf{u}| |\boldsymbol{\omega}| \rangle$ where $H = \langle \mathbf{u} \cdot \boldsymbol{\omega} \rangle$ is the flow net helicity), two flows were considered as initial conditions: the Taylor-Green (TG) flow [5], and the Arn'old-Beltrami-Childress (ABC) flow [6]. The TG flow is non-helical, and has zero energy in the $k_z = 0$ mode, whose amplification observed in the rotating cases (see below) is thus only due to a cascade process. The TG flow was chosen for its importance in hydrodynamics; it was originally motivated as an initial condition which leads to rapid development of small spatial scales. It also mimics the von Kármán flows between two counter-rotating disks used in several experiments. The ABC

flow is an eigenfunction of the curl operator and as a result has maximum helicity. It was used as a paradigmatic example to study helical flows in the atmosphere [1]. Both flows develop, after a short time, an infrared energy spectrum proportional to k^2 ; this is important to ensure we can compare the decay rates of both flows.

The simulations were started using a superposition of these flows from wavenumbers $k = 4$ to 14. Runs with zero relative helicity have a superposition of TG flows and runs with $h \approx 0.95$ have a superposition of ABC flows. The initial energy spectrum from $k = 4$ to 14 was proportional to k^{-4} , leaving enough spectral space to allow for direct and inverse transfer of energy. All the runs were extended for over 40 turnover times, and the dissipative range was properly resolved. Times in Table I and in the figures are expressed in units of the turnover time at $t = 0$, $T = L/U$, where $L \approx 2\pi/k_0 = 2\pi/4$ is the initial integral scale of the flow and $U \approx 1$ is the initial r.m.s. velocity.

Several Reynolds, Rossby, and Ekman numbers can be defined for the runs. We will consider here the Reynolds number based on the integral scale $Re = UL/\nu$, and the accompanying Rossby number $Ro = U/(2\Omega L)$. The integral scale is defined as $L = 2\pi \int E(k)k^{-1}dk/E$ where $E(k)$ is the isotropic energy spectrum and E is the total energy. The Ekman number is then defined as $E_k = Ro/Re$. At $t = 0$ runs in set A have $Re = 1047$ and runs in set B have $Re = 2244$. At the same time the Rossby number is $Ro = 0.08$ for runs A3, A4, and B1-B2; the initial Ekman number is then $E_k = 7.6 \times 10^{-5}$ in runs A3 and A4, and $E_k = 3.6 \times 10^{-5}$ in runs B1-B2. Values of the controlling parameters for each run at the time of maximum dissipation t^* are given in Table I.

It is also convenient to introduce a micro-scale Rossby number as $Ro^\omega = \omega/(2\Omega)$ [7]. This number can be interpreted as the ratio of the convective to the Coriolis acceleration at the Taylor scale, a scale characteristic of the turbulent inertial range. In order for anisotropies to develop in the simulations, the Rossby number Ro must be small enough for the rotation to affect the free decaying turbulence, but the micro-Rossby Ro^ω must be larger than one for scrambling effects of inertial waves not to completely damp the nonlinear terms (which leads to a pure exponential viscous decay) [8]. We are thought interested in simulations with moderate rotation rates to ensure $Ro \lesssim 1$ and with Re large enough to have enough scale separation between the energy-containing and the dissipative scale. Note in Table I how Ro and Ro^ω are one order of magnitude apart in all runs at time t^* . This difference is sustained in time in the runs during the self-similar energy decay.

Figure 1 shows the time history of the energy and enstrophy in runs A1, A2, B1-B2. In all runs there is a self-similar decay after the time t^* . Runs A3 and A4 (not shown) decay respectively as runs B1 and B2, although the time span of the self-similar stage is shorter. In both runs with $\Omega = 0$, the energy decays as $\sim t^{-2}$. As will be discussed later, this exponent corresponds to the

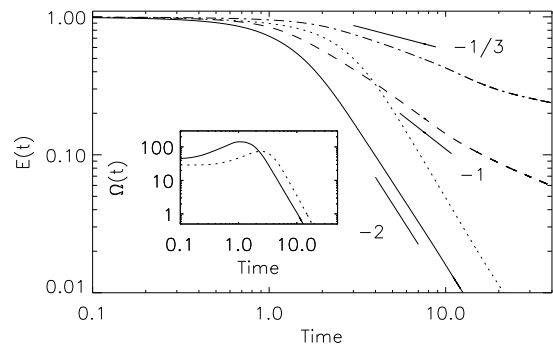


FIG. 1: Energy evolution for runs A1 (solid), A2 (dotted), B1 (dashed) and B2 (dot-dashed). Runs A1 and A2 have $\Omega = 0$ and decay with the same rate independently of the helicity content. When rotation is turned on the decay rates differ. Inset: enstrophy evolution for runs A1 and A2.

decay of a flow with constant integral length [9].

The presence of helicity in run A2 doesn't seem to affect the self-similar decay of turbulence, as predicted in Ref. [10]. This is in good agreement with the fact that helicity doesn't change the spectral index of the energy in non-rotating turbulence [2]. However, the self-similar decay in run A2 starts at a later time, as also previously reported in Ref. [11]. This is associated with the slowdown in the generation of small-scales in helical flows [12], which results in a longer time to reach the maximum of dissipation in run A2 (see the inset in Fig. 1).

In runs with rotation (A3, A4, B1 and B2), a transient is also observed before t^* . Then, self-similar decays with different power laws for the energy are found in all runs. Runs A3 and B1 have a decay near t^{-1} [13, 14], while the runs with maximum helicity (A4 and B2) follow a decay slightly faster than $t^{-1/3}$. Contrary to the non-rotating case, we can appreciate now how the presence of initial helicity changes the self-similar energy decay.

The time evolution is accompanied by a change in the shape of the energy spectrum (see Fig. 2(a)). While the runs without rotation show at t^* and during the self-similar decay an spectrum consistent with Kolmogorov scaling in both the energy and the helicity, runs with rotation show different scaling laws. Run B1 (which has a larger scale separation than run A3) shows an isotropic energy spectrum compatible with k^{-2} (the anisotropic energy spectrum is also compatible with a k_{\perp}^{-2} scaling) [17, 18]. On the other hand, the energy spectrum in run B2 is slightly steeper than in run B1, while the helicity spectrum in this run is shallower than the energy spectrum. The product of both spectra is consistent with a k^{-4} scaling law, as predicted using phenomenology for rotating helical flows in [18].

In the runs with rotation, a change in the small-scale spectrum is observed at $t \approx 20$. As energy piles up at the largest available scale in the box and column-like structures form in the velocity, the small-scale energy spec-

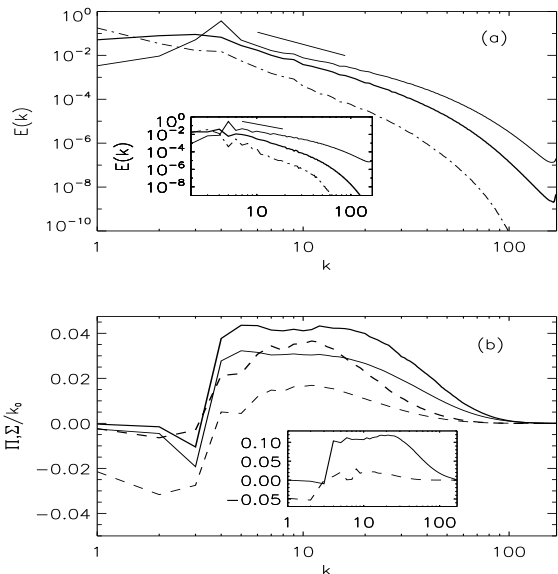


FIG. 2: (a) Isotropic energy spectrum for run B2 at times $t \approx 2$ (thin), $t \approx 12$ (thick) and $t \approx 30$ (dot-dashed). At early times the spectrum follows a $\sim k^{-2.5}$ power-law (slope shown as a reference) and becomes later dominated by the piling up of energy in the large scales. Inset: Isotropic energy spectrum for run B2. A k^{-2} slope is plotted for reference. (b) Energy (thin) and helicity (thick) normalized fluxes for run B2 at times $t \approx 5$ (solid) and $t \approx 13$ (dashed) respectively. Inset: Energy flux for run B1 at times $t \approx 2$ (solid) and $t \approx 11$ (dashed).

trum becomes steeper. This is accompanied by a decrease in the decay rate of the energy (see Fig. 1). This process is reminiscent of the change observed in the free-decay of two-dimensional turbulence, when the coalescence of large-scale vortices at late times leads to a steeper energy spectrum and a change in the self-similar decay [16]

Runs A1 and A2 develop direct energy fluxes toward small-scales while the rotating non-helical runs (A3 and B1) show both a direct and an inverse energy cascade (see the inset of Fig. 2 (b)). In the helical runs (Fig. 2 (b)), at $t \approx 2$ we observe maximum flux of energy and helicity toward smaller scales, evidencing both energy and helicity have a direct cascade. However, the helicity flux is larger than the direct energy flux. Later, an inverse cascade of energy can be clearly identified from the negative energy flux at large scales. At $t \approx 13$, the coexistence of both an inverse cascade of energy and direct cascades of energy and helicity is observed.

Although Figs. 2 (a) and (b) show the isotropic spectra and fluxes, the flows in the rotating case are anisotropic. Most of the energy in the spectra is in modes perpendicular to the axis of rotation, and the anisotropic spectrum $E(k_{\perp})$ and flux $\Pi(k_{\perp})$ look similar to the ones previously discussed. We present instead some global indications of the development of anisotropies. Figure 3 shows the ratio of the energy in perpendicular modes

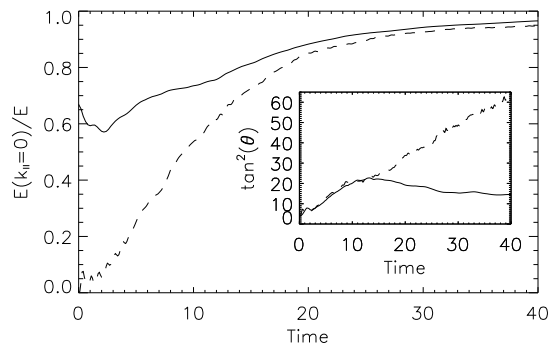


FIG. 3: Ratio of the energy in modes with $k_{\parallel} = 0$ to the total energy in runs B1 (dashed) and B2 (solid). Despite the different initial conditions, the curves grow monotonically to 1, showing a transfer of energy to perpendicular modes. Inset: time evolution of the Shebalin angle for the same runs.

(i.e., modes with $k_{\parallel} = 0$) to the total energy in runs B1 and B2. Differences at early times are due to different initial conditions. However, it can be seen that both curves grow monotonically to a value near 1, indicating the flows evolve toward anisotropic states as the energy is transferred to perpendicular modes [3].

A measure of anisotropies in the small-scale fluctuations is given by the Shebalin angle, defined as

$$\tan^2 \theta = 2 \frac{\sum_{k=1}^{k_{max}} k_{\perp}^2 E(k_{\perp})}{\sum_{k=1}^{k_{max}} k_{\parallel}^2 E(k_{\parallel})}, \quad (2)$$

The evolution of this angle in runs B1 and B2 can be seen in the inset of Fig. 3. It grows monotonically although in run B2 it reaches a maximum at $t \approx 12$ and then seems to saturate. A similar behavior is observed for L_{\parallel} (not shown) which again grows monotonically in B1 but reaches a maximum in B2 at approximately the same time. In all cases, $\tan^2 \theta \gg 2$ which corresponds to anisotropic flows.

The increase of the correlation lengths, together with the growth of $E(k_{\parallel} = 0)/E$ and of $\tan^2 \theta$ speaks of anisotropization of the flows. This tendency towards two-dimensionalization is confirmed by exploring the flows in real space. Fig. 4 shows visualizations of the r.m.s. vorticity with superimposed velocity field lines for runs A3 and A4 at late times ($t \approx 45$). In both cases, a strong anisotropy is observed with large scale column-like structures in the vorticity (similar structures are observed if energy density is visualized instead). However, a significant difference in the geometry of the flow in the columns is observed between runs A3 and A4. While the flow in the columns of the helical run is strongly helical (the flow goes either up or down in the entire column, thus giving helical velocity field lines), the columns of the non-helical run have no net helicity (the flow goes up and down inside the same column). This indicates that even at late times, the properties of the emerging structures in rotat-

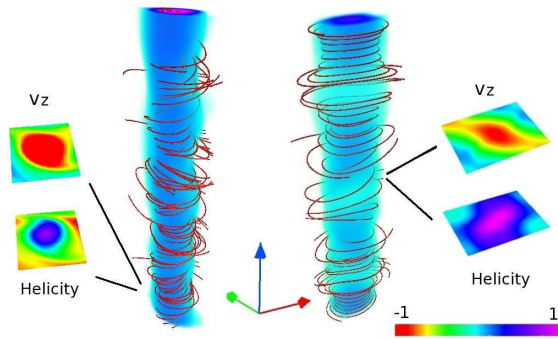


FIG. 4: (Color online) Visualizations of the r.m.s. vorticity for $t \approx 45$ with superimposed velocity field lines for runs A3 (right) and A4 (left). Cuts of v_z and H on a plane perpendicular to Ω are shown. The color table gives the amplitudes normalized to the maximum of each quantity.

ing flows depend on the initial helicity content.

The results presented so far show a novel and distinct evolution in the free decay of helical and non-helical flows when rotation is present. These differences can be understood in terms of a simple phenomenological theory. For the non-rotating cases we make use of the classical Kolmogorov phenomenology which leads to the well known energy spectrum $E(k) \sim \epsilon^{2/3} k^{-5/3}$, where ϵ represents the energy dissipation rate. From the Navier-Stokes equation it is easy to show that for a freely-decaying flow $dE/dt \sim E^{3/2}/L$ which leads to a self-similar decay law $E(t) \sim t^{-2}$ if the integral scale is assumed constant [4, 9].

In the case of rotating non-helical flows, it is often assumed that $E(k) \sim \epsilon^{1/2} \Omega^{1/2} k^{-2}$ (for simplicity, we use

the isotropic wavenumber k , although the arguments here can be easily generalized to the anisotropic case replacing k by k_{\perp}). This spectrum was observed in simulations [17], and obtained from closures [14]. It can also be derived from phenomenological arguments assuming the inertial waves slow down the energy cascade [19]. Using this spectrum it follows that $dE/dt \sim (E/L)^2$ resulting in a decay law $E(t) \sim t^{-1}$.

The novel case of rotating helical flows differs from the previous two cases. The direct transfer is dominated by the helicity cascade. Writing the helicity flux as $\delta \sim h_l/(\Omega\tau_l^2)$ where h_l is the helicity at the scale l and τ_l the eddy turnover time, leads to spectra $E(k) \sim k^{-n}$ and $H(k) \sim k^{n-4}$, where $n = 5/2$ for the case of maximum helicity [18]. In this case, dimensional analysis leads to $E(t) \sim \epsilon^{1/4} \Omega^{5/4} k^{-5/2}$ and to $E(t) \sim t^{-1/3}$. Note that for flows with initial helicity between zero and the maximum, the decay rate is between -2 and $-1/3$. A run with relative helicity of $h \approx 0.4$ was done to verify this.

The results indicate that helical and non-helical rotating flows differ in their scaling laws and decay rates. This is different than the case of non-rotating flows where helicity doesn't change the energy scaling. The observed differences indicate that helical rotating flows must be studied in detail, and open new directions in the study of rotating turbulence. This can also be the starting point to elucidate the actual role helicity plays in the decay of flows in nature where rotation is often relevant [1].

Computer time provided by NCAR and CECAR. The authors acknowledge support from grant UBACYT X468/08. PDM is a member of the Carrera del Investigador Científico of CONICET. Flow visualizations were done using VAPOR [20].

-
- [1] D.K. Lilly, *Atm. Sc.* **40**, 126 (1986).
[2] V. Borue and S.A. Orszag, *Phys. Rev. E* **55**, 7005 (1997); Q. Chen, S. Chen, and G.L. Eyink, *Phys. Fluids* **15**, 361 (2003); P. D. Mininni, A. Alexakis, and A. Pouquet, *Phys. Rev. E* **74**, 016303 (2006).
[3] C. Cambon and L. Jacquin, *J. Fluid Mech.* **202**, 295 (1989); F. Waleffe, *Phys. Fluids A* **5**, 677 (1993); C. Cambon, N.N. Mansour, and F.S. Godeferd, *J. Fluid Mech.* **337**, 303 (1997).
[4] P.G. Saffman, *Phys. of Fluids* **10**, 1349 (1967); U. Frisch, *Turbulence: The legacy of A.N. Kolmogorov* (Cambridge Univ. Press, Cambridge, 1995); L. Skrbek and S.R. Stalp, *Phys. Fluids* **12**, 1997 (2000); P.A. Davidson, *Turbulence* (Oxford University Press, 2004).
[5] G.I. Taylor and A.E. Green, *Proc. Roy. Soc. Lond. Ser. A* **158**, 895 (1937), 499.
[6] S. Childress and A.D. Gilbert, (*Stretch, Twist, Fold: The fast dynamo*) (Springer-Verlag Berlin, 1995).
[7] L. Jacquin *et al.*, *J. Fluid Mech.* **220**, 1 (1990).
[8] C. Cambon, N.N. Mansour, and F.S. Godeferd, *J. Fluid Mech.* **337**, 303 (1997).
[9] L. Biferale *et al.*, *Phys. Fluids* **15**, 2105 (2003).
[10] R.H. Kraichnan, *J. Fluid Mech.* **59**, 745 (1973).
[11] Y. Morinishi, K. Nakabayashi, and S. Ren, *JSME Int. J. Ser. B* **44**, 410 (2001).
[12] J.C. André and M. Lesieur, *J. Fluid Mech.* **81**, 187 (1977).
[13] P.A. Davidson, P.J. Staplehurst, and S.B. Dalziel, *J. Fluid Mech.* **557**, 135 (2006); C. Morize and F. Moisy, *Phys. Fluids* **18**, 065107 (2006).
[14] F. Bellet *et al.*, *J. Fluid Mech.* **562**, 83 (2006).
[15] P.D. Mininni and A. Pouquet, *Phys. Rev. Lett.* **99**, 254502 (2007).
[16] J.C. McWilliams, *J. Fluid Mech.* **146**, 21 (1984).
[17] W.C. Müller and M. Thiele, *Europhy. Lett.* **77**, 34003 (2007); P.D. Mininni, A. Alexakis, and A. Pouquet, *Phys. Fluids* (in press) arXiv:0802.3714v1 (2008).
[18] P.D. Mininni and A. Pouquet, (submitted to *Phys. Rev. E*), arXiv:0707.3620v1 (2008).
[19] Y. Zhou, *Phys. Fluids* **7**, 2092 (1995).
[20] J. Clyne *et al.*, *New J. Phys.* **9**, 301 (2007).